PAPER

New insights into the comprehension of the magnetic properties of dinuclear Mn^{III} compounds with the general formula [{MnL(NN)}$_2$(μ-O)(μ-n-RC$_6$H$_4$COO)$_2$]X$_2$†

Luis Escriche-Tur,*[a,b] Mercè Font-Bardia,[c] Belén Albela[b] and Montserrat Corbella*[a,d]

Five new dinuclear Mn(III) compounds with benzoato derivative bridges [{Mn(bpy)L}$_2$(μ-O)(μ-n-RC$_6$H$_4$COO)$_2$]X$_2$ (n-R = 3-MeO, 4-MeO and 4-tBu, X = NO$_3^-$ and ClO$_4^-$) were synthesised and characterised. According to X-ray diffraction, the X anions tend to be coordinated to the Mn ions and may occupy the place of the monodentate ligand L. Two structural isomers that only differ in one of their monodentate ligands have been obtained with the 3-MeOC$_6$H$_4$COO$^-$ bridges. For all compounds, the Mn(III) ions display elongated octahedra with a pronounced rhombic distortion. To quantify these distortions separately, the elongation and rhombicity parameters Δ and ρ have been defined. The magnetic study shows a good relationship between the distortion of the coordination polyhedra and the zero field splitting parameters (D_{Mn} and E_{Mn}). From the magnetic data of a powder sample, it is possible to determine the sign and magnitude of D_{Mn} for ferromagnetic systems or weak antiferromagnetic systems with $D_{Mn} < 0$. For this kind of dinuclear compound, the R group at the *meta* position, the rhombic distortion of the octahedra, and large torsion angles between the Jahn–Teller axes lead to ferromagnetic interactions.

Introduction

The interest in the magnetic properties of dinuclear Mn^{III} compounds with the [Mn$_2$(μ-O)(μ-R'COO)$_2$]$^{2+}$ core lies in the versatility of their magnetic behaviour, which ranges from moderate ferro- to antiferromagnetic, with a ground state $S = 4$ and $S = 0$, respectively. The Mn ions in these compounds show an octahedral geometry with pronounced axial and rhombic distortions. The axial distortion is distinctive of Mn^{III} ions, the octahedra can be elongated in the direction of the terminal ligands or compressed in the direction of the oxo bridging ligand. In general, those compounds that have compressed octahedra display ferromagnetic coupling, while those with elongated octahedra show antiferromagnetic coupling. When the predominant distortion is rhombic, the interaction may be either ferro- or antiferromagnetic.[1–5]

Compounds with tridentate amines as blocking ligands usually display compressed distortion and, accordingly, a significant ferromagnetic interaction is observed.[1,6–9] Nevertheless, some compounds displaying rhombic distortion may also be found, which show a weak antiferromagnetic interaction.[10,11]

When the capping ligand is bidentate, such as 2,2′-bipyridine (bpy) or 1,10-phenanthroline (phen), the sixth position of the coordination octahedra is occupied by a monodentate ligand, which provides greater flexibility in the coordination environment and gives distortions of different types and degrees.[2] However, there is only one compound displaying compressed octahedra around the Mn(III) ions, [{Mn(bpy)(N$_3$)}$_2$(μ-O)(μ-C$_6$H$_5$COO)$_2$], and it shows an important ferromagnetic coupling.[12,13] The rest of them display elongated coordination octahedra toward the monodentate ligands. However, the magnitude of this distortion is sensitive to the specific monodentate ligand and its donor or acceptor character.[2,4]

In the last few years, we have focussed our attention on the study of the magnetic properties of this kind of dinuclear

[a]Departament de Química Inorgànica i Orgànica (Secció inorgánica), Universitat de Barcelona, C/Martí i Franquès 1-11, 08028 Barcelona, Spain.
E-mail: luis.escrichetur@gmail.com, montse.corbella@qi.ub.es
[b]Laboratoire de Chimie, ENS de Lyon, Université de Lyon, 46 Allée d'Italie, 69364 Lyon Cedex 07, France
[c]Cristal·lografia, Mineralogia i Dipòsits Minerals, Universitat de Barcelona, Martí i Franquès s/n, 08028 Barcelona, Spain
[d]Institud de Nanociència i Nanotecnologia de la Universitat de Barcelona (IN²UB), Av. Joan XXIII s/n, 08028 Barcelona, Spain

compound with benzoate-derivative bridges[2–4,14,15] and the factors that determine the magnetic interaction. The interest is centred on the structural changes promoted by the monodentate ligand and the steric hindrance due to the substituent of the benzoato derivative. The analysis of the magnetic properties of compounds with 2-$RC_6H_4COO^-$ bridging ligands showed that the magnetic interaction for this kind of compound also depends on the relative orientation of the Jahn–Teller axes of the Mn^{III} ions and the planarity between the aromatic ring and the carboxylate group.[2]

Furthermore, the magnetic anisotropy or zero-field splitting (ZFS) is one of the most important properties that characterises a metal ion with $S > 1/2$.[16] Particularly, the Mn^{III} ion is known to display significant axial (D) and rhombic (E) anisotropy parameters.[17] The ZFS has been studied on several occasions for mononuclear compounds, providing an idea about the nature and magnitude of these parameters.[16–19] Nevertheless, the determination of the single-ion anisotropy for polynuclear compounds is very challenging, since the overall magnetic properties are dependent on both the isotropic ($Mn\cdots Mn$ interactions) and the asymmetric interactions (referred to as ZFS).[16,20]

In this work we analyse the magnetic properties of a family of seven compounds with the general formula [{Mn(bpy)L}$_2$-(μ-O)(μ-n-RC_6H_4COO)$_2$]X$_2$, where n-R = 2-MeO (**1** and **2**), 3-MeO (**3**, **4**, and **5**), 4-MeO (**6**), or 4-^tBu (**7**), X = NO_3 (**1**, **3**, and **4**) or ClO_4 (**2**, **5**, **6**, and **7**), and L = H_2O, EtOH, or X. Compounds **1** and **2** were recently published, but a deep discussion of their magnetic properties was not reported.[21] The crystal structures of the new compounds (**3–7**) are reported here. The magnetic coupling constant and the ZFS parameters of the Mn^{III} ions have been determined and the limits of detection for the sign and magnitude of these parameters have been evaluated. Moreover, the analysis of the structural parameters and the magnetic data of twenty-six analogous compounds has been carried out with the aim to find the ligands that could contribute to obtain systems with a ground state $S = 4$.

Experimental

Synthesis

All manipulations were performed under aerobic conditions. Reagents and solvents were obtained from commercial sources and used without further purification. NBu_4MnO_4 was prepared as described in the literature.[22]

Caution! Perchlorate salts of compounds containing organic ligands are potentially explosive. Only small quantities of these compounds should be prepared.

[{Mn(bpy)(NO₃)}₂(μ-3-MeOC₆H₄CO₂)₂(μ-O)]·H₂O (3·H₂O). 3-MeOC₆H₄CO₂H (1.6 mmol, 0.24 g) and Mn(NO₃)₂·4H₂O (1.28 mmol, 0.32 g) were dissolved in acetonitrile. Then, a pre-filtered acetonitrile solution (10 mL) of NBu_4MnO_4 (0.32 mmol, 0.12 g) was added to the previous solution in small portions over 1–2 minutes while, almost simultaneously, an acetonitrile solution (10 mL) of 2,2′-bipyridine (bpy)

(1.6 mmol, 0.25 g) was added, also in small portions. The resulting black solution (total volume ∼25 mL) was stirred for 10–15 minutes and shortly afterward filtered to separate any possible precipitate. After keeping the solution in a refrigerator for one day, dark crystals were collected by filtration. Yield: 67%. Anal. Calcd for $C_{36}H_{30}Mn_2N_6O_{13}\cdot H_2O$ (M.W. = 882.55) (%): C, 48.99; H, 3.65; N, 9.52. Found (%): C, 47.71; H, 3.67; N, 9.16. Selected IR data (cm⁻¹): 3388 (br), 3088 (w), 2999 (w), 2929 (w), 2837 (w), 1610 (m), 1560 (s), 1497 (w), 1471 (w), 1448 (m), 1383 (vs), 1300 (s), 1282 (s), 1245 (s), 1155 (w), 1107 (m), 1082 (w), 1043 (s), 1032 (s), 919 (w), 902 (m), 876 (w), 762 (s), 728 (s), 681 (w), 662 (w), 653 (w), 634 (w), 445 (m), 415 (w).

[{Mn(bpy)(H₂O)}{μ-3-MeOC₆H₄CO₂)₂(μ-O){Mn(bpy)(NO₃)}]-NO₃·1/2H₂O·1/2MeCN (4·1/2H₂O·1/2MeCN). An analogous procedure was followed as for **3**, but using 50 mL of acetonitrile and adding 1 mL of H_2O over 5 min after the addition of all reagents. After three days in the refrigerator, dark crystals were collected by filtration. Yield: 55%. Anal. Calcd for $C_{36}H_{32}Mn_2N_6O_{14}\cdot1/2MeCN\cdot1/2H_2O$ (M.W. = 912.08) (%): C, 48.72; H, 3.81; N, 9.98. Found (%): C, 49.07; H, 3.79; N, 9.87. Selected IR data (cm⁻¹): 3397 (br), 3107 (w), 3078 (w), 3059 (w), 3031 (w), 3003 (w), 2973 (w), 2938 (w), 2836 (w), 1601 (m), 1561 (s), 1496 (w), 1466 (w), 1446 (m), 1384 (vs), 1320 (s), 1279 (m), 1248 (s), 1166 (m), 1117 (w), 1103 (w), 1047 (w), 1054 (w), 1032 (s), 993 (w), 916 (w), 884 (w), 833 (w), 728 (m), 762 (s), 727 (s), 664 (w), 645 (w), 456 (w, br), 412 (w).

[{Mn(bpy)(H₂O)}{μ-3-MeOC₆H₄CO₂)₂(μ-O){Mn(bpy)(ClO₄)}]-ClO₄·3H₂O (5·3H₂O). 3-MeOC₆H₄CO₂H (1.6 mmol, 0.24 g) and Mn(ClO₄)₂·6H₂O (1.32 mmol, 0.46 g) were dissolved in acetonitrile. Then, solid NBu_4MnO_4 (0.32 mmol, 0.12 g) was added to the previous solution in small portions over 1–2 minutes while, almost simultaneously, an acetonitrile solution (10 mL) of 2,2′-bipyridine (bpy) (1.6 mmol, 0.25 g) was added, also in small portions. The resulting black solution (total volume ∼20 mL) was stirred for 15 minutes. Afterwards, the volume was reduced to 5 mL using a rotary evaporator (35 °C, 0.2 Bar) and filtered to separate any possible residue. The solution was layered with n-hexane (10 mL) and CH_2Cl_2 (5 mL). After four days, dark crystals were isolated by filtration and dried under vacuum. Yield: 65%. Anal. Calcd for $C_{36}H_{32}Cl_2Mn_2N_4O_{16}\cdot3H_2O$ (M.W. = 1011.48) (%): C, 42.75; H, 3.79; N, 5.54. Found (%): C, 43.04; H, 3.77; N, 5.34. Selected IR data (cm⁻¹): 3420 (br), 3106 (w), 3091 (w), 3065 (w), 2972 (w), 2940 (w), 2840 (w), 1608 (m), 1560 (s), 1496 (w), 1471 (m), 1448 (s), 1381 (s), 1313 (m), 1280 (m), 1248 (m), 1106 (vs), 1032 (vs), 917 (w), 886 (w), 786 (m), 754 (s), 728 (s), 663 (w), 623 (m), 545 (w, br), 459 (m), 415 (w).

[{Mn(bpy)(EtOH)}{μ-4-MeOC₆H₄CO₂)₂(μ-O){Mn(bpy)(ClO₄)}]-ClO₄·1/3MeCN·1/3H₂O (6·1/3MeCN·1/3H₂O). 4-MeOC₆H₄CO₂H (1.6 mmol, 0.24 g) and Mn(ClO₄)₂·6H₂O (1.32 mmol, 0.46 g) were dissolved in acetonitrile. Then, a pre-filtered acetonitrile solution (10 mL) of NBu_4MnO_4 (0.32 mmol, 0.12 g) was added to the previous solution in small portions over 1–2 minutes while, almost simultaneously, an acetonitrile solution (10 mL) of 2,2′-bipyridine (bpy) (1.6 mmol, 0.25 g) was added, also in small portions. The resulting black solution (total volume ∼30 mL) was stirred and reduced to ∼6 mL. This solution was

mixed with absolute ethanol (20 mL) and filtered to separate any possible residue. Tiny black crystals were obtained after two days in the refrigerator. Yield: 45%. Anal. Calcd for $C_{38}H_{36}Cl_2Mn_2N_4O_{16} \cdot 1/3MeCN \cdot 1/3H_2O$ (M.W. = 1005.18) (%): C, 46.20; H, 3.78; N, 6.04; Cl, 7.05. Found (%): C, 46.67; H, 3.80; N, 6.16; Cl, 7.08. Selected IR data (cm^{-1}): IR (cm^{-1}): 3364 (br), 3113 (w), 3086 (w), 2957 (w), 2930 (w), 2901 (w), 2836 (w), 1604 (s), 1552 (s), 1497 (w), 1470 (m), 1446 (m), 1417 (m), 1391 (s), 1313 (m), 1255 (s), 1171 (s) 1103 (s, br), 1049 (s), 926 (w), 853 (w), 784 (m), 765 (m), 729 (m), 662 (w), 623 (s), 512 (w), 415 (m).

$[\{Mn(bpy)(EtOH)\}(\mu\text{-}4\text{-}^tBuC_6H_4CO_2)_2(\mu\text{-}O)\{Mn(bpy)(ClO_4)\}]ClO_4$ (7). $4\text{-}^tBuC_6H_4CO_2H$ (1.6 mmol, 0.28 g) and $Mn(ClO_4)_2 \cdot 6H_2O$ (1.28 mmol, 0.46 g) were dissolved in absolute ethanol (10 mL). Next, solid NBu_4MnO_4 (0.32 mmol, 0.12 g) was added to the previous solution in small portions over 1–2 minutes while, almost simultaneously, 10 mL of an absolute ethanol solution of 2,2′-bipyridine (bpy) (1.6 mmol, 0.25 g) was added, also in small portions. The resulting black solution (total volume ~20 mL) was stirred for 15 minutes and shortly afterward filtered in order to separate any possible precipitate. The solution was left undisturbed in a refrigerator for a week. Dark crystals were isolated by filtration, washed with ethanol and dried under vacuum. Yield: 32%. Anal. Calcd for $C_{44}H_{48}Cl_2Mn_2N_4O_{14}$ (M.W. = 1037.65) (%): C, 50.93; H, 4.66; N, 5.40. Found (%): C, 50.32; H, 4.49; N, 5.52. Selected IR data (cm^{-1}): 3366 (br), 3116 (w), 3087 (w), 3054 (w), 2962 (m), 2910 (w), 2867 (w), 1611 (m), 1588 (m), 1548 (m), 1499 (w), 1472 (m), 1448 (m), 1382 (s), 1313 (w), 1270 (w), 1250 (w), 1195 (w) 1107 (s), 1032 (s), 922 (w), 862 (w), 789 (m), 777 (m), 748(w), 730 (m), 711 (m), 664 (w), 620 (m), 544 (w), 476 (w), 418 (w).

X-ray crystallography

The data collection for compounds **3**, **4**, **5** and **7** was carried out at 100 K on a Bruker Apex-II diffractometer, whereas for **6**, it was carried out at 273 K on a MAR345 diffractometer, both equipped with graphite monochromated Mo Kα radiation (λ = 0.71073 Å). Cell parameters were refined by the least-squares method using around 9900 reflections. Between 29 302 and 123 002 reflections were collected using the Φ- and ω-scan (Bruker Apex-II) or Φ-scan (MAR345) method. Data were corrected for absorption effects using the multi-scan (**3**, **5** and **7**) or empirical (**4** and **6**) method (SADABS).[23] Table S1† summarises crystallographic data collection and structure refinement details.

The structures were solved by direct methods and refined by full-matrix least-squares using SHELXL-97.[24] Non-hydrogen atoms were refined anisotropically, whereas hydrogen atoms were computed and refined with isotropic thermal parameters riding on their respective carbon or oxygen atoms.

Compound **3**·2CH$_3$CN crystallises in the monoclinic space group $C2/c$. The asymmetric unit consists of half of the neutral complex $[\{Mn(bpy)(NO_3)\}_2(\mu\text{-}3\text{-}MeOC_6H_4CO_2)_2(\mu\text{-}O)]$ located on a 2-fold rotation axis and a molecule of acetonitrile. A total of 286 parameters were refined in the final refinement on F^2 using no restraints.

Compound **4**·1/2H$_2$O·1/2MeCN crystallises in the triclinic space group $P\bar{1}$. The asymmetric unit consists of a cationic complex $[\{Mn(bpy)(H_2O)\}(\mu\text{-}3\text{-}MeOC_6H_4CO_2)_2(\mu\text{-}O)\{Mn(bpy)(NO_3)\}]^+$, a nitrate anion, a 50% occupancy acetonitrile molecule and a 50% occupancy water molecule. A total of 556 parameters were refined in the final refinement on F^2 using 63 restraints.

Compound **5** crystallises in the triclinic space group $P\bar{1}$. The asymmetric unit consists of a cationic complex $[\{Mn(bpy)(H_2O)\}(\mu\text{-}3\text{-}MeOC_6H_4CO_2)_2(\mu\text{-}O)\{Mn(bpy)(ClO_4)\}]^+$, a perchlorate anion and disordered molecules of solvent. The program SQUEEZE (part of the PLATON package of crystallographic software)[25] was used to calculate the solvent disorder and remove its contribution to the overall intensity data.[26] Fifty-one electrons were found in a 161 Å^3 void, corresponding to the diffuse contribution of a dichloromethane and a water molecule. A total of 592 parameters were refined in the final refinement on F^2 using 286 restraints.

Compound **6**·1/3MeCN·1/3H$_2$O crystallises in the trigonal space group $R\bar{3}$. The asymmetric unit consists of a $[\{Mn(bpy)(H_2O)\}(\mu\text{-}3\text{-}MeOC_6H_4CO_2)_2(\mu\text{-}O)\{Mn(bpy)(ClO_4)\}]^+$ complex, a perchlorate anion and disordered acetonitrile (on the 3-fold axis) and water molecules (around and on the 3-fold axis). A total of 591 parameters were refined in the final refinement on F^2 using 38 restraints.

Compound **7** crystallises in the orthorhombic space group $Pca2(1)$. The asymmetric unit consists of two conformational isomers of the cationic complex $[\{Mn(bpy)(EtOH)\}(\mu\text{-}4\text{-}^tBuC_6H_4CO_2)_2(\mu\text{-}O)\{Mn(bpy)(ClO_4)\}]^+$ and two perchlorate anions. A total of 1244 parameters were refined in the final refinement on F^2 using 480 restraints.

Physical characterisation

Chemical analyses (C, H, N and Cl) were carried out by the "Centres Científics i Tecnològics" of the Universitat de Barcelona and by the "Servei de Microanàlisi" of the "Consell Superior d'Investigacions Científiques (CSIC)". Infrared spectra were recorded on KBr pellets in the 4000–400 cm^{-1} range with a Thermo Nicolet Avatar 330 FTIR spectrometer. Magnetic susceptibility (χ_M) measurements (2–300 K) were carried out in a Quantum Design MPMS XL5 SQUID Magnometer at the Unitat de Mesures Magnètiques (Universitat de Barcelona), using a field of 200 G. Pascal's constants were used to estimate the diamagnetic corrections for each compound. Magnetisation measurements were carried out in the range 1.8–6.8 K and at six different magnetic fields (0.5, 1.0, 2.0, 3.0, 4.0 and 5.0 T).

Results and discussion

Synthesis

The synthetic method used to obtain the dinuclear Mn^{III} compounds **3–7** consists of a comproportionation reaction between Mn^{II} and MnO$_4^-$ in the presence of a benzoic derivative acid and 2-2′-bipyridine (bpy), which leads to compounds with the

general formula $[\{Mn(bpy)(L)\}(\mu\text{-}n\text{-}RC_6H_4CO_2)_2(\mu\text{-}O)\{Mn(bpy)\text{-}(L')\}]X_{2-m}$, where $n\text{-}R$ = 3-MeO (**3–5**), 4-MeO (**6**) or 4-^{t}Bu (**7**) and X = NO_3 (**3** and **4**) or ClO_4 (**5–7**). L and L′ are monodentate ligands that can be H_2O, EtOH or X. If both positions (L and L′) are occupied by X, like in compound **3**, a neutral complex is formed. In the rest of compounds (**4–7**), only one of the monodentate positions is occupied by the anion X, so the complex is a monovalent cation. The syntheses and crystal structures of compounds with $n\text{-}R$ = 2-MeO (**1** and **2**) were recently published.[21] The synthesis of compounds with X = NO_3 and $n\text{-}R$ = 4-MeO and 4-^{t}Bu was also previously reported, but no X-ray suitable crystals were obtained.[14]

The perchlorate compounds (**5–7**) are much more soluble than nitrate compounds (**3** and **4**) in acetonitrile solution, as reported before for analogous compounds with $n\text{-}R$ = 2-Me and $n\text{-}R$ = 2-F.[4] Thus, while the nitrate compounds (**3** and **4**) could be crystallised from the acetonitrile solution, the perchlorate compounds (**5–7**) did not crystallise from the mother liquor. Compound **5** was obtained by slow diffusion of n-hexane (precipitant) into an acetonitrile solution of **5** layered with CH_2Cl_2. Compounds **6** and **7** are insoluble in ethanol solution, so they were crystallised by mixing a very concentrated solution of acetonitrile mother liquor with ethanol (**6**) or using ethanol instead of acetonitrile in the synthesis (**7**).

The IR spectra of these compounds show several characteristic bands assigned to the asymmetric and symmetric vibrations of the carboxylate groups ($\sim$1560 and 1365 cm^{-1}, respectively), the bypyridine ($\sim$1600, 1498, 1480 and 1450 cm^{-1}) and the Mn–O–Mn group ($\sim$730 cm^{-1}). The value $\Delta\nu = \nu_a(COO) - \nu_s(COO) \approx 200$ cm^{-1} is indicative of carboxylate ligands coordinated in bidentate bridging mode ($\mu_{1,3}$).[27] Compounds (**5–7**) display a strong band at $\sim$1110 cm^{-1} and a medium band at $\sim$620 cm^{-1}, both assigned to the perchlorate anion. Compounds **3** and **4** display an intense band at $\sim$1352 cm^{-1} corresponding to the nitrate anion, which overlaps the $\nu_s(COO)$.

Compounds **3** and **4** are structural isomers that only differ from one of the monodentate ligands (**3**, L = L′ = NO_3; **4**, L = H_2O and L′ = NO_3) and are obtained under very similar conditions. However, the presence of water in the mother liquor favours the formation of **4**, whereas **3** is obtained in dry acetonitrile. Fortunately, these two compounds can be easily differentiated by the shape of their crystals (Fig. S1†) and their IR spectra in the 960–800 cm^{-1} window (Fig. S2†). While **3** crystallises as big blocks and displays a band centred at 902 cm^{-1} of moderate intensity and two weak ones at 919 and 876 cm^{-1}, **4** crystallises as small star-shaped agglomerations of needles and shows a pair of bands at 916 and 884 cm^{-1}. To determine the suitable conditions to obtain the two compounds separately, several syntheses were performed controlling the addition of water. A pure sample of **3** was only isolated when dry acetonitrile was used. On the other hand, **4** was crystallised with a H_2O/MeCN volume ratio of 0.02. Note that higher ratios than this are unnecessary and lead to the decomposition of the Mn compound. If H_2O vapour diffusion is used as a crystallisation method, a

mixture of the two compounds was obtained, indicating that humidity should be controlled. Hence, it is convenient to observe the sample under a magnifying glass to ensure the purity of the sample.

Description of structures

The crystal structures of compounds **3–7** are shown in Fig. 1. In all these compounds, the two Mn^{III} ions show a distorted octahedral environment and are linked by one oxo and two $\mu_{1,3}\text{-}n\text{-}RC_6H_4COO^-$ bridges. Each manganese ion is bound to a 2,2′-bipyridine (bpy) ligand, and the hexacoordination of each Mn ion is completed by a monodentate ligand. In compound **3**, the monodentate ligands are nitrate anions, so the resulting complex is neutral. In compounds **4–7**, one of the monodentate ligands is a NO_3^- (**4**) or a ClO_4^- anion (**5–7**) and the other one is a water molecule (**4** and **5**) or EtOH (**6** and **7**), resulting in a cationic complex.

The Mn⋯Mn distance is $\sim$3.15 Å and the Mn–O_b–Mn angle is $\sim$123°. The Mn–O_b bond distances of the oxo bridges are $\sim$1.78 Å and the Mn–N distances are $\sim$2.06 Å. The carboxylate ligands are coordinated in a *syn–syn* conformation mode. One of the oxygen atoms is placed *trans* to the monodentate ligand, with a Mn–O_t distance of $\sim$2.16 Å, whereas the other oxygen atom is placed in a *cis* position, with a shorter Mn–O_c distance ($\sim$1.96 Å). The Mn–L bond lengths of the monodentate ligands are the largest in the first coordination sphere and are in the range 2.17–2.48 Å. Selected interatomic distances for these compounds are listed in Table S2† (for **3**), Table S3† (for **4–6**) and Table S4† (for **7**). More particular details concerning the structures and intermolecular interactions may be found in the ESI.†

The structural parameters of these compounds are in agreement with those reported for compounds with the same $[Mn_2(\mu\text{-}O)(\mu\text{-}n\text{-}RC_6H_4CO_2)_2]^{2+}$ core.[2,4,5,14,15,21,28] However, it is worth remarking that **6**, with a Mn2–O7 of 2.48 Å (Mn–O_{ClO_4}), has the longest Mn–L bond distance found for this kind of compound.

In these five compounds, the carboxylate group and the aromatic ring of the benzoate derivative are almost coplanar, having a twist angle $\omega(O\text{-}C_{carb}\text{-}C_{ar}\text{-}C'_{ar})$ in the range of 0–17°. The relative orientation of the two coordination octahedra is near perpendicularity, with the torsion angle $\tau(L\text{-}Mn\cdots Mn\text{-}L)$ between 68 and 117°. The values of these angles are also in agreement with those reported for compounds with *meta-* and *para*-benzoate derivatives (n = 3 and 4).[5,14,28] In contrast, compounds with *ortho*-benzoate derivatives (n = 2) usually show higher ω values.[2,4,15]

As mentioned before, all Mn^{III} ions in these compounds display elongated octahedra along the monodentate ligand direction; thus, the Jahn–Teller elongation axes should be approximately situated on the O_t–Mn–L direction. Besides, they also show a rhombic distortion (the Mn–O_b bond distance is significantly smaller than Mn–O_c). Considering the z axis in the O_t–Mn–L direction and the x axis in the oxo-bridge direction (Fig. 2), approximate values of the octahedron axis lengths can be found by addition of Mn-ligand distances:
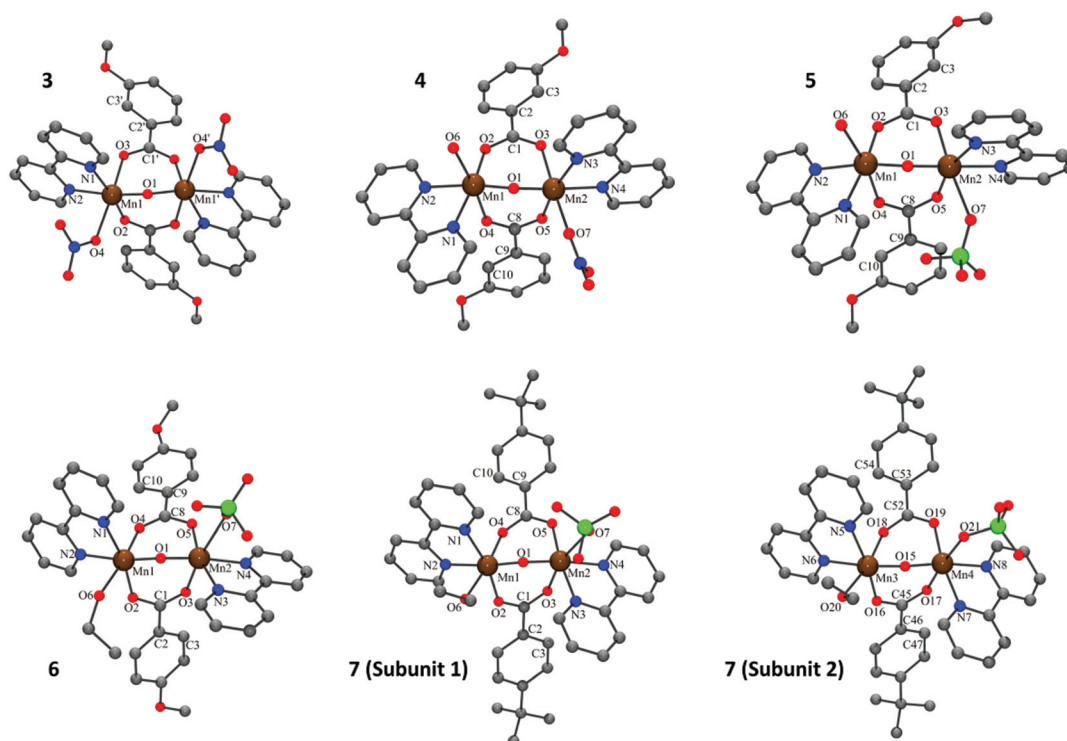
Fig. 1 Crystal structures of compounds **3–7**. Hydrogen atoms were omitted for clarity. Colour code: Mn, brown; C, grey; O, red; N, blue; Cl, green.
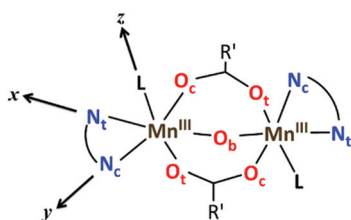

Fig. 2 Schematic representation of the structure of the dinuclear Mn^{III} complexes with the axes of the octahedron.

$x = d(\text{Mn–O}_b) + d(\text{Mn–N}_t)$, $y = d(\text{Mn–O}_c) + d(\text{Mn–N}_c)$ and $z = d(\text{Mn–L}) + d(\text{Mn–O}_t)$.

Formerly, G. Fernández *et al.* described the distortion parameter $(\lambda)^4$ as $\lambda = (z - y)/(y - x)$ and it was used for several series of compounds.[2,5,14] This parameter, which normally ranges from 0.2 to 3.5, offers the possibility to identify the predominant distortion (elongated octahedron if $\lambda > 2$, rhombic distortion if $2 > \lambda > 1$, compressed octahedron if $\lambda < 1$). However, it does not allow us to quantify both distortions separately, which could be essential to better rationalise the axial and rhombic anisotropies of the Mn^{III} ions (see below). In addition, λ shows an overstatement of the elongation when the rhombic distortion is very small. For instance, the Mn2 ion in **6** shows a very small rhombic distortion ($x \approx y$); so, the λ parameter becomes enormous (value of 10) compared to the other Mn^{III} ions in compounds **1–5, 7** (values between 1.3 and 3.8) (see Table 1).

Table 1 *x*, *y* and *z* axes lengths and the elongation (Δ), rhombicity (ρ), and distortion (λ) parameters of each Mn ion for compounds **1–7**

		x/Å	*y*/Å	*z*/Å	Δ/%	ρ/%	λ
1	Mn1	3.846	4.037	4.367	10.80	4.97	1.73
2	Mn1	3.844	4.021	4.396	11.79	4.60	2.12
	Mn2	3.845	4.006	4.42	12.60	4.19	2.57
3	Mn1	3.8558	4.0194	4.4255	12.39	4.24	2.48
4	Mn1	3.841	4.063	4.353	10.15	5.78	1.31
	Mn2	3.833	4.009	4.451	13.52	4.59	2.51
5	Mn1	3.8546	4.0331	4.3373	9.98	4.63	1.70
	Mn2	3.8406	4.0039	4.5362	15.65	4.25	3.26
6	Mn1	3.8209	4.0201	4.4436	13.34	5.21	2.13
	Mn2	3.8733	3.9398	4.6048	17.87	1.72	10.0
7	Mn1	3.849	4.003	4.375	11.44	4.00	2.42
	Mn2	3.827	3.97	4.507	15.61	3.74	3.76
	Mn3	3.84	3.999	4.373	11.57	4.14	2.35
	Mn4	3.838	4.006	4.472	14.02	4.38	2.77
Average		**3.84**	**4.01**	**4.43**			
S		**0.01**	**0.03**	**0.08**			

$x = d(\text{Mn–O}_b) + d(\text{Mn–N}_t)$; $y = d(\text{Mn–O}_c) + d(\text{Mn–N}_c)$; $z = d(\text{Mn–O}_L) + d(\text{Mn–O}_t)$; $\Delta = (z - \overline{xy})/\overline{xy}$, $\overline{xy} = (x + y)/2$; $\rho = (y - x)/x$; s = standard deviation.

Hence, in order to quantify both distortions, we defined two parameters for the elongation (Δ) and rhombicity (ρ) with the following formulae:

$$\Delta = \frac{z - \overline{xy}}{\overline{xy}} \tag{1}$$

$$\rho = \frac{y - x}{x} \tag{2}$$

where $\overline{xy} = (x + y)/2$. While Δ represents how different the Jahn–Teller axis is from the average length between x and y axes, ρ represents the distortion within the xy plane. Both parameters are dimensionless and can be expressed in the form of percentage for better clarity. For all these compounds (1–7), Δ should be greater than ρ ($\Delta > \rho$) and both of them should be positive, characteristic of elongated octahedra with small or moderate rhombic distortion. This model can also be applied to compressed octahedra, in this case $\Delta < 0$. In both kinds of octahedra, $|\Delta| > |\rho|$ (the absolute value of the elongation parameter should be greater than the absolute value of the rhombic one). If $|\Delta| < |\rho|$, the axes are improperly assigned. And if $|\Delta| \approx |\rho|$, the octahedron has a pronounced rhombic distortion or the axes are improperly assigned.

The axis length and the Δ and ρ parameters for compounds 1–7 are listed in Table 1. Note that the average values of the axes follow the trend $z > y > x$ with their respective standard deviations (s) following the trend $s_z > s_y > s_x$, which indicates that the length for the z axis is the most variable. The resulting Δ and ρ distortions are in the ranges 10.0–17.9% and 1.7–5.8%, respectively; and, in accord with that explained above, these values are consistent with elongated octahedra with different degrees of rhombic distortion.
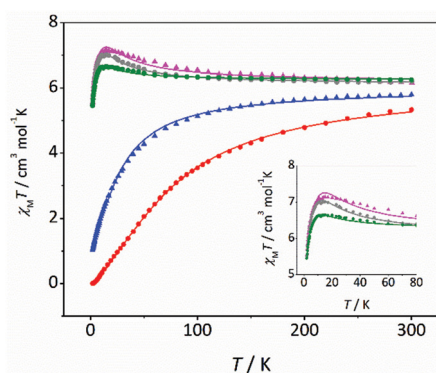

Fig. 3 $\chi_M T$ vs. T plots for compounds **3** (pink triangles), **4** (grey circles), **5** (green circles), **6** (blue triangles) and **7** (red circles). The solid lines are the best fits of the experimental data.

Magnetic properties

Magnetic susceptibility (χ_M) data were recorded for compounds **3–7** from 300 to 2 K. $\chi_M T$ vs. T plots for **3–7** are shown in Fig. 3. Note that the curves are remarkably different. The $\chi_M T$ values at room temperature are between 5.3 and 6.3 cm^3 mol^{-1} K, which are close to the expected value for two uncoupled Mn^{III} ions. For compounds **3–5**, the $\chi_M T$ values remain almost constant until 100 K; but they increase below this temperature, reaching maximum values of 7.1 (**3**), 7.0 (**4**) and 6.7 (**5**) cm^3 mol^{-1} K at ~13 K. This behaviour is indicative of a ferromagnetic coupling (spin ground state $S = 4$). Below 13 K, $\chi_M T$ values slightly decrease due the zero-field splitting, as expected for Mn^{III} ions. On the other hand, for compounds **6** and **7**, the $\chi_M T$ values decrease as the temperature falls (more pronouncedly in the case of **7**), indicative of an antiferromagnetic coupling (spin ground state $S = 0$). However, these compounds show different behaviour at very low temperature: for **7** the $\chi_M T$ reaches zero, characteristic of an isolated singlet ground state; while for **6** the $\chi_M T$ value at 2 K is 0.9 cm^3 mol^{-1} K, indicating a non-negligible population in the first excited states. The magnetic study for compounds **1** and **2** was recently reported.[21] Both compounds present a weaker antiferromagnetic coupling than **6** and **7**, and show deviations in the low temperature range of the $\chi_M T$ vs. T plot, similar to **6**.

$\chi_M T$ vs. T data of compound **7** were fitted with the PHI program,[29] considering the Heisenberg spin Hamiltonian $H = -2JS_1S_2$, whose results are presented in Table 2. On the other hand, the magnetic data of compounds **3–6** could not be fitted considering an isotropic system, as also happened with the aforementioned compounds **1** and **2**.[21] Indeed, it was necessary to include the ZFS parameters to fit the experimental $\chi_M T$ vs. T data of compounds **3–6**.

The zero-field splitting (ZFS) effect removes the degeneration of the M_S states of each S level, and the energy gap between the M_S states (D_S and E_S) depends on the magnitudes and signs of the anisotropy parameters of the Mn^{III} ions, D_{Mn} and E_{Mn}.[30] In the case of Mn^{III} ions with elongated octahedral geometry like in compounds **3–7**, negative and moderate values of D_{Mn} are expected.[16–19] The low symmetry of the octahedra in these compounds also causes a pronounced rhombic distortion; so, significant E_{Mn} values are also expected.[18,19] In addition, D_{Mn} and E_{Mn} are directional and,

Table 2 List of magnetic parameters obtained from the fit of $\chi_M T$ vs. T and $M/N\mu_\beta$ vs. H plots

Ref.	G	$2J^a$/cm^{-1}	$D_{Mn}{}^b$/cm^{-1}	$E_{Mn}{}^c$/cm^{-1}	$E_{Mn}/|D_{Mn}|$	$R_{SUS}(R_{MAG})^d$
1[21]	2.01	−2.3	−4.6	+1.0^e	0.22	3.1×10^{-5} (3.0×10^{-3})
2[21]	2.01	−0.7	−3.0	—	—	9.0×10^{-5} (1.1×10^{-3})
3	2.04	+1.8	−5.1	+1.1	0.22	1.3×10^{-4} (2.5×10^{-4})
4	2.02	+1.3	−4.1	+1.1	0.27	2.3×10^{-5} (3.4×10^{-4})
5	2.04	+0.52	−3.1	+0.66	0.21	2.4×10^{-5} (9.5×10^{-4})
6	2.00	−4.8	−5.3	+1.0^e	0.19	3.1×10^{-4} (4.3×10^{-3})
7	2.04	−16.0	—	—	—	1.5×10^{-4} (—)

^{a} Referred to the spin Hamiltonian $H = -2JS_1 \cdot S_2$. ^{b} ZFS parameter related to the axial anisotropy. ^{c} ZFS parameter related to the rhombic anisotropy. ^{d} $R_{SUS} = \sum[(\chi_M T)_{exp} - (\chi_M T)_{calcd}]^2/\sum[(\chi_M T)_{exp}]^2$; $R_{MAG} = \sum[(M/N\mu_\beta)_{exp} - (M/N\mu_\beta)_{calcd}]^2/\sum[(M/N\mu_\beta)_{exp}]^2$. ^{e} Kept constant.

consequently, their relative orientation may affect the ZFS of each state (D_S and E_S). Particularly for the compounds presented here, D_{Mn} vectors should be approximately located along the z axis according to Fig. 2. Hence, their relative orientation (β angle) may have a pronounced effect on the M_S splitting, since they would be around orthogonality ($\beta \approx 90°$). This can affect the low temperature range of the $\chi_M T$ vs. T plot if there is any populated state with $S \neq 0$. So, this could have some influence for compounds with weak or moderate antiferromagnetic magnetic interactions.

With the aim to see the effect of the relative disposition of the distortion axes, several simulations of the $\chi_M T$ vs. T plot were carried out with fixed values of $2J$ and D_{Mn}, but modifying the β angles between 0 and 90°. As it could be expected, for systems with strong antiferromagnetic interactions the effect of the β angle on the $\chi_M T$ vs. T plot is negligible. However, for systems with weak and moderate antiferromagnetic interactions, a significant effect on the shape of the graph was observed. Fig. 4 shows the $\chi_M T$ vs. T plot for systems with $2J = \pm 1$ cm^{-1} and $D_{Mn} = -4$ cm^{-1}. For the antiferromagnetic system with parallel Jahn–Teller axes ($\beta = 0$), $\chi_M T$ values fall to zero at low temperature, as expected for a ground state $S = 0$; however, when the axes are orthogonal ($\beta = 90°$), a significant deviation of the graph is observed.

It is well known that for systems with ferromagnetic interaction, the ZFS of the ground state $S = 4$ justifies the decay of the $\chi_M T$ values at low temperatures. This effect is influenced by the relative orientation of the Jahn–Teller axes (as in antiferromagnetic compounds): the $\chi_M T$ maximum shifts to a higher temperature and the $\chi_M T$ value of the maximum decreases for $\beta = 90°$.

To acquire more information, magnetisation (M) data were collected for compounds **3–6** in the range 1.8–6.8 K, applying magnetic fields between 0.5 and 5.0 T. $M/N\mu_\beta$ vs. HT^{-1} plots for compounds **4–6** are shown in Fig. 5 and S7.† The non-super-
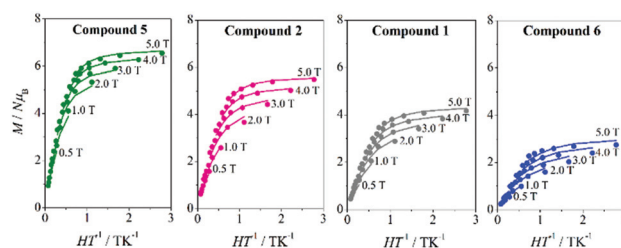

Fig. 5 $M/N\mu_\beta$ vs. HT^{-1} plots for **5** (green), **2**[21] (pink), **1**[21] (grey), and **6** (blue). The solid lines are the best fits of the experimental data.

position of the various isofield lines is indicative of a significant ZFS. All plots present similar features, without showing saturation at the highest field and lowest temperature, with maximum $M/N\mu_\beta$ values around $6N\beta$ for the ferromagnetic compounds **3–5** and $2.8N\beta$ for the antiferromagnetic compound **6**. For compound **7**, which shows $\chi_M T$ values close to zero at low temperature, no significant magnetisation signal can be expected.

The question arises whether one can determine the sign of ZFS parameters by fitting $\chi_M T$ vs. T and $M/N\mu_\beta$ vs. HT^{-1} plots and upon the precision of the results obtained from these fits. To solve these matters, several simulations of the $\chi_M T$ vs. T and $M/N\mu_\beta$ vs. HT^{-1} plots were performed by screening different $2J$ and D_{Mn} values, all of them considering a relative orientation of the Jahn–Teller axes $\beta = 90°$.

For compounds with antiferromagnetic coupling ($S = 0$ ground state), the effect of the D_{Mn} parameter can only be observed if the first excited state ($S = 1$) is populated; for moderate or strong antiferromagnetic interactions ($|2J| > 6$ cm^{-1}), the population of this excited state at low temperature is almost negligible and the effect of the D_{Mn} parameter is unnoticed. The ZFS of the $S = 1$ state strongly depends on the D_{Mn} parameter, since $|D_{S=1}| = 4.2|D_{Mn}|$.

For compounds with ferromagnetic coupling ($S = 4$ ground state), the effect of the D_{Mn} parameter is always observable because it affects the ground state. However, for the same D_{Mn} value, the ZFS of the $S = 4$ ($D_{S=4}$) is much smaller than the ZFS of the $S = 1$ ($|D_{S=1}| = 10|D_{S=4}|$ for parallel Jahn–Teller axes).

When the anisotropy parameter (D_{Mn}) is small, ($|D_{Mn}| \leq 2$ cm^{-1}), the effect of their magnitude and sign on the $\chi_M T$ vs. T and $M/N\mu_\beta$ vs. HT^{-1} plots is unimportant; although its effect could be noticed in the $M/N\mu_\beta$ vs. HT^{-1} plot, the assignment of the sign of D_{Mn} would be ambiguous. On the other hand, for greater $|D_{Mn}|$ values the differences between the plots simulated with positive and negative D_{Mn} values become more relevant as $|D_{Mn}|$ increases.

The information obtained from each one of these plots complements the other one. Magnetisation plots are very sensitive to the magnitude and sign of D_{Mn}, except for compounds with moderate–strong antiferromagnetic coupling. However, the quantification of the magnetic coupling constant ($2J$) should not be performed using this plot. The $\chi_M T$ vs. T plot is, contrary to the previous one, highly affected by the $2J$ value,
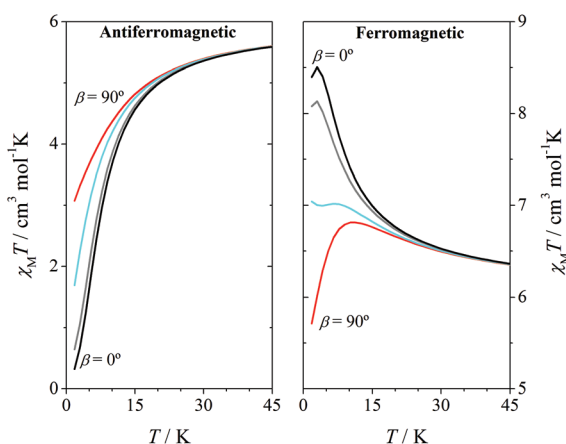

Fig. 4 Effect of the relative orientation of axial anisotropy axes (β) on the $\chi_M T$ vs. T plots of a hypothetical Mn$_2^{III}$ compound with $g = 2.0$, $2J = \pm 1.0$ cm^{-1}, $D_{Mn} = -4.0$ cm^{-1} and $\beta = 0°$ (black), 30° (grey), 60° (cyan) and 90° (red); considering the Hamiltonian $H = -2JS_1S_2$.

but the D_{Mn} parameter only affects in the low temperature range. For compounds with weak antiferromagnetic interactions, different behaviour could be observed as a function of the sign of D_{Mn}. When $D_{Mn} > 0$, $\chi_M T$ values tend to zero upon cooling and, consequently, the D_{Mn} value cannot be determined from these data; whereas, when $D_{Mn} < 0$, the $\chi_M T$ vs. T plot shows a deviation at low temperature ($\chi_M T$ values do not reach zero) and the magnitude of D_{Mn} should have some influence on the fitting of the experimental data. For ferromagnetic compounds, the $\chi_M T$ vs. T plots show differences depending on the magnitude of D_{Mn}, but the effect of the sign is sometimes insignificant.

To sum up, the determination of the magnitude and sign of the ZFS parameters of the single ion (D_{Mn}) can only be performed for compounds displaying ferromagnetic or weak antiferromagnetic coupling. For a good accuracy it is necessary to fit the $\chi_M T$ vs. T and $M/N\mu_\beta$ vs. HT^{-1} data simultaneously, the first allows the determination of the magnetic coupling constant ($2J$) and the magnetisation data allow the determination of the ZFS parameters of the single ions (D_{Mn}).

Therefore, the $\chi_M T$ vs. T and $M/N\mu_\beta$ vs. HT^{-1} plots of compounds **3–6** were fitted simultaneously using the PHI program ($H = -2JS_1S_2$),[29] considering the zero-field splitting (ZFS) parameters of manganese ions (D_{Mn} and E_{Mn}) and a relative orientation of the Jahn–Teller axes of 90°. Table 2 shows the results for the best fit of the experimental data for compounds **3–7**. Compounds **3–6** and those reported previously (**1** and **2**) show negative values of D_{Mn}. Particularly for compounds **1**, **2**, and **6**, with a weak antiferromagnetic behaviour, the sign and magnitude of the D_{Mn} are relevant for both the $\chi_M T$ vs. T and $M/N\mu_\beta$ vs. HT^{-1} plots. Moreover, the values obtained for D_{Mn} are consistent with elongated Mn^{III} ions with distorted octahedral geometry, which typically give moderate and negative D_{Mn}.[16–19] The $E_{Mn}/|D_{Mn}|$ ratios, which are in the range 0.19–0.27, are in agreement with elongated octahedra with rhombic distortion ($x \neq y$). Furthermore, a good correlation between the $E_{Mn}/|D_{Mn}|$ ratio and the rhombic distortion (ρ) is found, as could be seen in Fig. 6. This highlights the importance of quantifying the axial and rhombic distortions of the Mn^{III} ions separately.

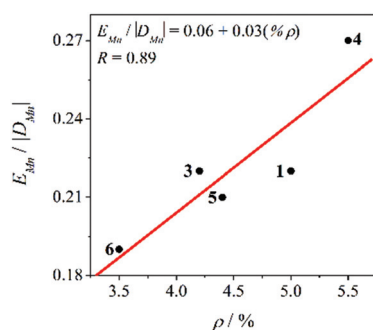**Fig. 6** $E_{Mn}/|D_{Mn}|$ ratio vs. rhombicity parameter (ρ) for compounds **1** and **3–6**. Compound **2** has not been included in this graph because its experimental data could have been fitted without considering the E parameter. The red line corresponds to the linear fit.

Magneto-structural correlations

Table 3 summarises the magnetic coupling constants and selected structural parameters for compounds **1–7** and nineteen other analogous compounds with benzoato derivative bridges ([{MnL(NN)}$_2$(μ-O)(μ-n-RC$_6$H$_4$COO)$_2$]X$_2$). As may be observed, the magnetic coupling constants for these compounds ($2J$) range from -16.0 to $+17.6$ cm^{-1}, compound **7** showing the most antiferromagnetic coupling. These compounds are classified according to the positions of the R group. As mentioned before, magneto-structural correlations for compounds with the R group at the *ortho* position ($n = 2$) had been reported previously.[2] The structural parameters analysed were the distortion of the octahedra, the relative orientation of both polyhedra and the twist angles between the benzoate ring and the COO group (Fig. 7). Now, the same structural parameters are analysed for compounds with the R group at the *meta* and *para* positions ($n = 3$ and 4, respectively).

In our previous work, we saw the influence of different structural parameters on the magnetic interaction individually.[2] Now, we would like to correlate these parameters aiming to find the one being more predominant for the magnetic interactions.

Distortion of octahedra (Δ and ρ). The compounds analysed here show elongated coordination octahedra with a significant rhombic distortion. Thus, their shape is governed by the parameters defined above, Δ and ρ. With the aim to improve the correlation between the distortion of the octahedra and the magnetic interaction, these parameters have been calculated for all the compounds reported in Table 3 from their crystal data. For all compounds except for **S**, the Mn^{III} ions display an elongated octahedral environment ($\Delta = 9.0$–15.6%) with notable rhombic distortion ($\rho = 3.5$–5.4%). Compound **S** (with L = N$_3$/N$_3$)[13] displays compressed octahedra towards the Mn–O$_{oxo}$ bond, therefore $\rho > \Delta$. In regard to the explanation above, the axial distortion of the manganese ions in this compound should be calculated considering the z axis in the direction of the Mn–O$_{oxo}$ bond, which would give $\Delta < 0$. Anyhow, we kept the definition of axes as presented in Fig. 2 in order to compare this compound with the rest.

In previous work[2–4] it was reported that the elongation of the octahedra is related to the antiferromagnetic behaviour. With the aim to see the effect of both distortion parameters on the magnetic coupling, Fig. 8 shows the contour plot of the rhombicity parameter (ρ) *versus* the elongation parameter (Δ) and the magnetic interaction ($2J$) for compounds collected in Table 3. Two facts can be deduced from this graph: firstly, the Δ and ρ parameters are inversely proportional; and, secondly, compounds with the ferromagnetic interaction show $\Delta \approx \rho$, while compounds with an antiferromagnetic interaction show $\Delta \gg \rho$. These results are consistent with those reported previously;[2] however, the new distortion parameters, which consider the elongation and the distortion of the xy plane separately, give a more accurate correlation.
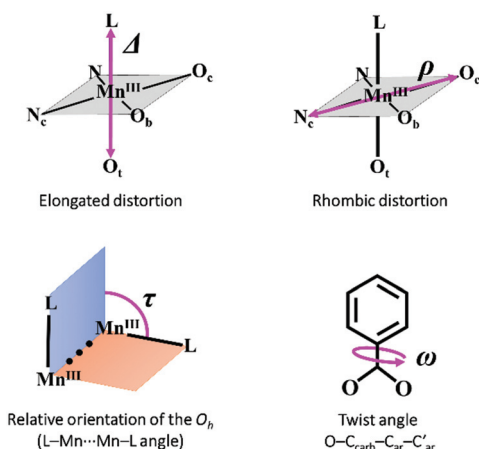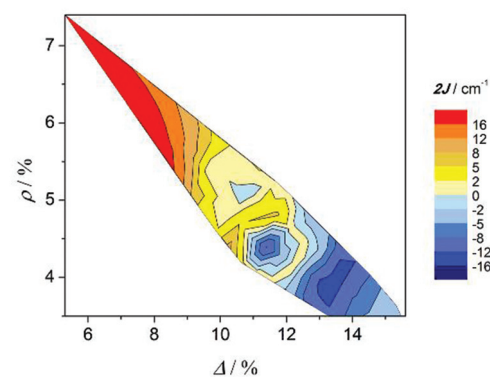
Table 3 Magnetic coupling constants 2J and selected structural parameters for [{MnL(NN)}$_2$(μ-O)(μ-n-RC$_6$H$_4$COO)$_2$]X$_2$ compounds

Ref.	n-R	NN	X	L	2J^a/cm⁻¹	Mn–O–Mn/°	Δ^b/%	ρ^c/%	ω^d/°	τ^e/°	γ^f/°
A[15]	2-Cl	Phen	ClO$_4$	H$_2$O/H$_2$O	−12.6	122.9	11.2	4.5	77.9	88.3	
B[2]	2-Cl	Bpy	ClO$_4$	H$_2$O/ClO$_4$ (3/1)	−10.9	122.8	13.3	3.5	56.5	92.6	
C[4]	2-Me	Bpy	ClO$_4$	H$_2$O/ClO$_4$	−5.6	122.3	13.8	3.7	46.9	101.1	
D[4]	2-F	Bpy	ClO$_4$	H$_2$O/ClO$_4$	−3.5	124.4	12.7	4.8	19.5	93.6	
1[21]	2-MeO	Bpy	NO$_3$	H$_2$O/NO$_3$	−2.3	123.5	10.8	5.0	36.2	78.1	0
2[21]	2-MeO	Bpy	ClO$_4$	H$_2$O/ClO$_4$	−0.7	122.8	12.2	4.4	29.2	95.2	
E[4]	2-Me	Bpy	NO$_3$	H$_2$O/NO$_3$	−0.5	123.1	10.7	4.2	28.8	97.2	79
F[2]	2-Cl	Phen	—	NO$_3$/NO$_3$	−0.3	124.4	9.7	4.7	38.1	101.7	22
G[4]	2-F	Bpy	NO$_3$	H$_2$O/NO$_3$	+1.4	125.1	11.2	5.0	18.6	89.2	18
H[15]	2-Cl	Phen	ClO$_4$	H$_2$O/H$_2$O	+2.7	122.9	9.7	4.9	46	102	
I[2]	2-Cl	Bpy	NO$_3$	H$_2$O/NO$_3$	+3.0	123.0	9.4	5.4	25.4	108.5	22
J[33]	2-COOH	Bpy	NO$_3$	H$_2$O/NO$_3$ (3/1)	+4.7	123.5	11.2	4.6	19.9	96.4	68
5	3-MeO	Bpy	ClO$_4$	H$_2$O/ClO$_4$	+0.5	123.9	12.8	4.4	10.7	102.3	
4	3-MeO	Bpy	NO$_3$	H$_2$O/NO$_3$	+1.3	124.7	11.8	5.2	11.8	92.8	8
3	3-MeO	Bpy	NO$_3$	NO$_3$/NO$_3$	+1.8	124.5	12.4	4.2	16.9	117.2	3
K[28]	3-Cl	Phen	ClO$_4$	H$_2$O/H$_2$O	+5.7	121.0	11.6	4.7	3.9	120.6	
L[28]	3-Cl	Bpy	NO$_3$	H$_2$O/H$_2$O	+11.8	122.4	9.0	5.4	5.8	112.7	
7	4-tBu	Bpy	ClO$_4$	EtOH/ClO$_4$	−16.0	120.8	13.2	4.1	3.8	73.7	
M[5]	4-Br	Bpy	ClO$_4$	EtOH/ClO$_4$	−6.8	122.8	14.6	4.0	10.7	94.1	
6	4-MeO	Bpy	ClO$_4$	EtOH/ClO$_4$	−5.2	123.5	15.6	3.5	11.7	95.5	
N[5]	4-Cl	Phen	ClO$_4$	EtOH/EtOH	0	122.1	11.1	4.1	6.7	88.9	
O[14]	4-F	Bpy	NO$_3$	H$_2$O/H$_2$O	+1.4	124.4	10.0	5.1	9.3	99	
P[14]	4-Me	Bpy	NO$_3$	H$_2$O/H$_2$O	+1.5	122.1	10.9	4.4	7.3	112	
Q[3]	H	Bpy	—	OH/NO$_3$	+2.0	124.1	10.8	5.3	10.2	94.9	8
R[14]	4-CF$_3$	Bpy	NO$_3$	H$_2$O/H$_2$O	+5.7	122.2	10.6	4.2	7.5	116	
S[13]	H	Bpy	—	N$_3$/N$_3$	+17.6	122.0	5.3	7.4	5.0	108.1	

^{a} $H = -2J(S_1 \cdot S_2)$. ^{b} Average elongation (eqn (1)): $\Delta = (z - \overline{xy})/\overline{xy}$, $\overline{xy} = (x + y)/2$. ^{c} Average rhombicity (eqn (2)): $\rho = (y - x)/x$. ^{d} Average O–C$_{carb}$–C$_{ar}$–C′$_{ar}$ angle. ^{e} Relative orientation of the O$_h$: L–Mn···Mn–L angle. ^{f} Mn–O–N–O torsion angle; abbreviations: bpy = 2,2′-bipyridine, phen = 1,10-phenanthroline.

Fig. 7 Structural parameters considered in the magneto-structural correlations for compounds with the formula [{MnL(NN)}$_2$(μ-O)(μ-n-RC$_6$H$_4$COO)$_2$]X$_2$.

Fig. 8 Magnetic coupling constant 2J vs. elongation parameter (Δ) and rhombicity parameter (ρ) for compounds with the formula [{MnL(NN)}$_2$(μ-O)(μ-n-RC$_6$H$_4$COO)$_2$]X$_2$.

Effect of the monodentate ligands. The effect of the monodentate ligands was concisely studied in some previous work.[2,5] As therein mentioned, compounds with L = ClO$_4$⁻ or EtOH show more elongated coordination octahedra than those with L = NO$_3$, and this fact favours the antiferromagnetic behaviour. A more accurate analysis of the effect of the L ligand on the magnetic interaction is reported here for the compounds collected in Table 3. To see the range of the elongation parameter (Δ) in relation to the monodentate ligand, these compounds may be classified depending on the couple of monodentate ligands present in the dinuclear entity: L = EtOH/ClO$_4$, H$_2$O/EtOH, H$_2$O/H$_2$O, H$_2$O/NO$_3$, and NO$_3$/NO$_3$. Compounds with L = H$_2$O/H$_2$O have been separated depending on their counter-anion (X). Fig. 9 shows the range of values for the elongation parameter (Δ) and for the magnetic coupling constant (2J) for the six groups of compounds.

Concerning the distortion parameter, compounds with perchlorate as the monodentate ligand display the largest elongations of the octahedra, Δ values being between 12 and 16%. This effect is magnified if they also contain ethanol. On
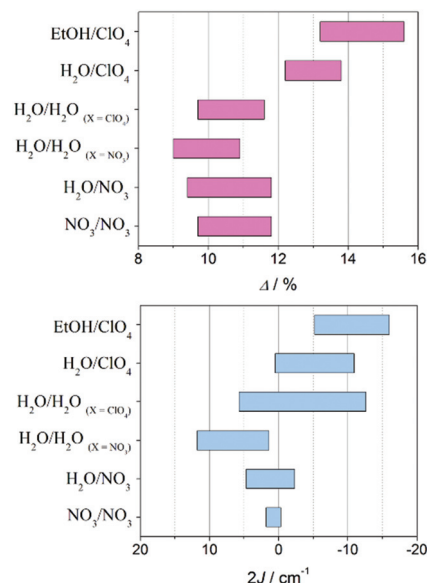
Fig. 9 Ranges for the elongation parameter Δ (top) and magnetic coupling constant J (bottom) for $[\{MnL(NN)\}_2(\mu\text{-}O)(\mu\text{-}n\text{-}RC_6H_4COO)_2]X_2$ compounds depending on their L ligand.

Fig. 10 Magnetic coupling constant $2J$ *vs*. the relative orientation of the octahedra (τ) and elongation parameter (Δ) for compounds with the formula $[\{MnL(NN)\}_2(\mu\text{-}O)(\mu\text{-}n\text{-}RC_6H_4COO)_2]X_2$.

the other hand, compounds containing water or nitrate show similar Δ values, but in a lower range (9–12%) than the ones with perchlorate.

Accordingly, compounds with perchlorate ligands show a more antiferromagnetic interaction than those with nitrate ligands. Surprisingly, compounds with L = H_2O/H_2O and perchlorate as counter-anions (non-coordinated) show more antiferromagnetic couplings than those with nitrate counter-anions, and this difference is more acute than that found for the elongation parameter (Δ). So, most compounds with the perchlorate ligand or counter-anion show antiferromagnetic behaviour, while compounds with the nitrate ligand or counter-anion show ferromagnetic behaviour. The cause of this fact may lie either in the resulting packing that each counter-anion provides or in the electronic effects promoted by hydrogen bonds $Mn\text{-}OH_2\cdots X$ (through the monodentate ligand).

Moreover, it was reported[4] that the magnetic interaction is also sensitive to the orientation of the nitrate ligand. When the NO_3^- ligand is positioned perpendicular to the z axis, with γ (MnONO torsion angle) close to 90°, it may act as a π-acid ligand and decreases the antiferromagnetic contributions. The three new compounds herein reported with the nitrate ligand (**1**, **3** and **4**) show a parallel disposition of these ligands, so we can expect a negligible π-acid effect of this ligand.

Relative orientation of octahedra, τ(L–Mn–Mn–L). Another parameter affecting the magnetic interaction is the relative orientation of the octahedra, defined as the torsion angle between monodentate ligands (τ). Aiming to see the relationship between this angle and the elongation parameter (Δ) and their influence on the magnetic interaction, a contour plot of these structural parameters (Δ and τ) and the magnetic
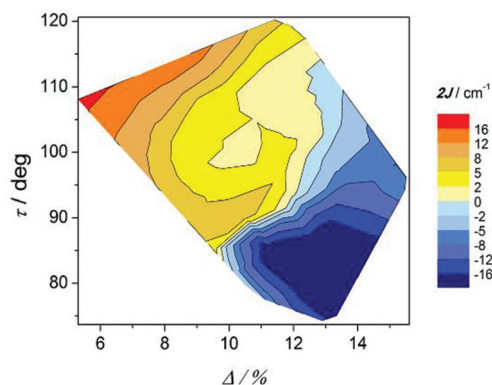
interaction is shown in Fig. 10. In general, compounds with elongated octahedra show minor values of the τ angles and show antiferromagnetic behaviour.

Twist angle $O\text{-}C_{carb}\text{-}C_{ar}\text{-}C'_{ar}$ (ω). This angle indicates the relative disposition of the COO group and the aromatic ring of the carboxylate bridging ligand: $\omega = 0°$, coplanar; 90°, orthogonal. This angle is very sensitive to the position of the R group of the carboxylate ligand. Fig. 11 shows the magnetic coupling constant *versus* this angle. For compounds with the R group at the *meta* and *para* positions ($n = 3$ and 4), this angle is in all cases small ($\omega < 20°$) and, thus, its effect on the magnetic interaction would be irrelevant. For compounds with the R group at the *ortho* position ($n = 2$) the values of this angle range from ~20 to ~88°, so, as it was reported previously,[2] this parameter has some influence on the magnetic properties. The ω value generally depends on the steric hindrance of the R group.

The correlation between this angle, the elongation parameter, and the magnetic interaction is shown in Fig. 12. As indicated, compounds with substantial elongation of the octahedra show antiferromagnetic behaviour. However, for
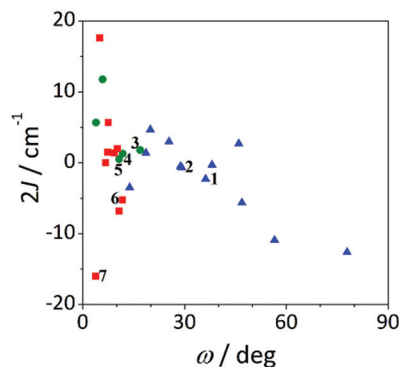

Fig. 11 Magnetic coupling constant $2J$ *vs*. twist angle $O\text{-}C_{carb}\text{-}C_{ar}\text{-}C'_{ar}$ (ω) for compounds with the formula $[\{MnL(NN)\}_2(\mu\text{-}O)(\mu\text{-}n\text{-}RC_6H_4COO)_2]X_2$ for $n = 2$ (blue triangles), 3 (green circles) and 4 (red squares).

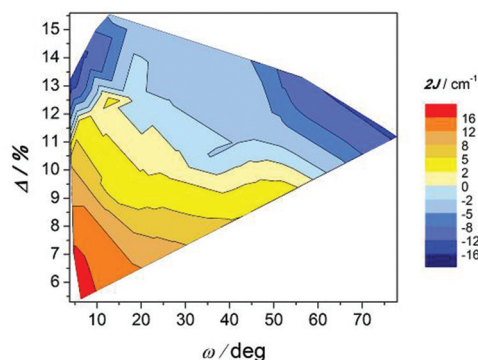**Fig. 12** Magnetic coupling constant $2J$ vs. twist angle $O-C_{carb}-C_{ar}-C'_{ar}$ (ω) and the elongation parameter (Δ) for compounds with the formula $[\{MnL(NN)\}_2(\mu-O)(\mu-n-RC_6H_4COO)_2]X_2$.

$\Delta > 10\%$ two regions where compounds display strong antiferromagnetic behaviour may be seen in the two extremes of the ω values.

The effect of the ω angle on the magnetic coupling has been reported for compounds **A** and **H**, two conformational isomers that have different ground states (spinomers). According to these theoretical studies, for $\omega \approx 0$ and 90°, the disposition of the orbitals of the carboxylate ligands is appropriate for overlapping with the d orbitals of the Mn ions; while for $\omega \approx 45°$, the topology of the orbitals changes and the antiferromagnetic contribution is reduced.[15] The results shown in Fig. 12 are in agreement with this study; for similar elongation values, the weaker antiferromagnetic behaviour is observed for a stacked configuration of the benzoate ring ($\omega \approx 40°$).

On the other hand, the most ferromagnetic compounds show small ω and Δ values; the slight elongation of the octahedra should be the major contribution to the ferromagnetic character.

The effect of the twist of the phenyl ring (ω) and the relative orientation of the octahedra (τ) on the magnetic coupling constant ($2J$) can be seen in Fig. 13. As in the precedent graph, two well defined regions with important negative $2J$ values are
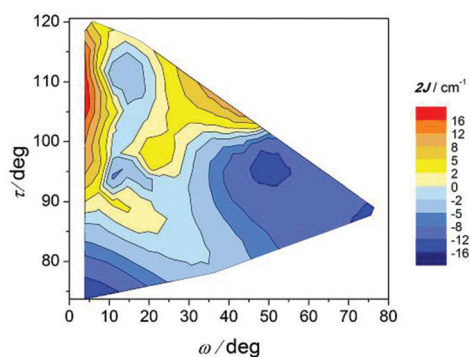
observed for τ angles below 100° at the two extremes of the ω values. For $\omega < 10°$, the magnetic interaction seems to be dictated by the τ angle, since the bigger this angle is, the more ferromagnetic the compound is. Nevertheless, as the phenyl ring loses the coplanarity with the COO group ($\omega > 10°$), ω becomes more relevant than τ for the magnetic coupling.

Electronic effect of the R group. The electron-donating character of the R group, as well as its position in the aromatic ring, could modify the electronic density on the Mn ions and, consequently, the magnetic coupling. It is interesting to highlight that the five compounds with the R group at the *meta* position (3-R) exhibit a ferromagnetic coupling, while compounds with the R group at the *para* or *ortho* position (4-R or 2-R) could show both magnetic behaviours. Moreover, with the 2-R group there are more compounds showing the antiferromagnetic interaction than the ferromagnetic interaction. The most relevant difference between the compounds with 3-R groups and compounds with 2-R or 4-R groups is in the relative disposition of the coordination octahedra (τ) that, in most cases, is greater than 100° for compounds with 3-R substituents.

Moreover, it was previously reported that, with similar structural parameters, compounds with an electron-withdrawing group show a more ferromagnetic behaviour than those with electron-donating groups.[14] The Hammett constant (σ) is related to the electronic effect of the R group, and has two contributions, due to the inductive and resonance effects.[31,32] Resonance contribution can only occur for substituents at the *ortho* and *para* positions. So, when the R group is at the *meta* position, the σ_{meta} only depends on the inductive effect. Moreover, inductive effects diminish with the distance between R and COO groups. Thus, for the same R group, σ_{meta} is generally greater than σ_{para} and, consequently, the 3-R group has a major electron-withdrawing character compared to the 4-R group.

Conclusions

Five new dinuclear Mn(III) compounds with benzoato derivative bridges $[\{Mn(bpy)L\}_2(\mu-O)(\mu-n-RC_6H_4COO)_2]X$ (n-R = 3-MeO, 4-MeO and 4-tBu) are reported. According to XRD, the X anions tend to be coordinated to the Mn ions and may occupy the place of the monodentate ligands L. Two structural isomers that only differ in their monodentate ligands have been obtained with the 3-MeOC$_6$H$_4$COO$^-$ ligand. For all compounds, the Mn^{III} ions show elongated octahedra with a pronounced rhombic distortion, the distortion axis being in the direction of the monodentate ligand. To quantify these distortions separately, the elongation and rhombicity parameters Δ and ρ have been defined.

The magnetic measurements revealed that compounds with n-R = 3-MeO display a ferromagnetic behaviour with the ground state $S = 4$, whereas compounds with n-R = 4-MeO and 4-tBu show an antiferromagnetic behaviour with the ground state $S = 0$. The Jahn–Teller axes of the Mn ions in these

Fig. 13 Magnetic coupling constant $2J$ vs. twist angle $O-C_{carb}-C_{ar}-C'_{ar}$ (ω) and relative orientation of the octahedra (τ) for compounds with the formula $[\{MnL(NN)\}_2(\mu-O)(\mu-n-RC_6H_4COO)_2]X_2$.

compounds are close to orthogonality and this fact has an important effect on the magnetic behaviour in the low temperature range for compounds with ferromagnetic or weak antiferromagnetic behaviour. Fitting all the magnetic data simultaneously, χ_M and M, makes it possible to determine the sign and magnitude of the ZFS parameters. For all compounds, D_{Mn} values are moderate and negative and the $E_{Mn}/|D_{Mn}|$ ratio is correlated with the rhombicity parameter (ρ).

Structural and magnetic data of twenty-six analogous compounds have been analysed and some new conclusions may be drawn:

(a) The elongation (Δ) and rhombicity (ρ) parameters are inversely proportional.

(b) The most elongated octahedra correspond to compounds with L = ClO_4 or EtOH. Consequently, compounds with L = EtOH/ClO_4 show the most antiferromagnetic behaviour.

(c) The torsion angle between the phenyl and the COO groups of the benzoic derivative (ω) is only important for compounds with the R group at the *ortho* position.

(d) The structural parameters leading to the ferromagnetic behaviour are rhombic distortion of the octahedra, coplanarity between the phenyl ring and the COO group, and a large angle between the Jahn–Teller axes.

(e) All compounds with the R group at the *meta* position (n = 3) exhibit ferromagnetism; this position provides a major electron-withdrawing character to the R group.

Acknowledgements

References

1 R. Hotzelmann, K. Wieghardt, U. Floerke, H. J. Haupt, D. C. Weatherburn, J. Bonvoisin, G. Blondin and J. J. Girerd, *J. Am. Chem. Soc.*, 1992, **114**, 1681–1696.

2 V. Gómez, M. Corbella, O. Roubeau and S. J. Teat, *Dalton Trans.*, 2011, **40**, 11968–11975.

3 M. Corbella, R. Costa, J. Ribas, P. H. Fries, J.-M. Latour, L. Öhrström, X. Solans and V. Rodríguez, *Inorg. Chem.*, 1996, **35**, 1857–1865.

4 G. Fernández, M. Corbella, G. Aullón, M. A. Maestro and J. Mahía, *Eur. J. Inorg. Chem.*, 2007, **2007**, 1285–1296.

5 M. Corbella, V. Gómez, B. Garcia, E. Rodriguez, B. Albela and M. A. Maestro, *Inorg. Chim. Acta*, 2011, **376**, 456–462.

6 C. Bolm, N. Meyer, G. Raabe, T. Weyhermüller and E. Bothe, *Chem. Commun.*, 2000, 2435–2436.

7 K. Wieghardt, U. Bossek, B. Nuber, J. Weiss, J. Bonvoisin, M. Corbella, S. E. Vitols and J. J. Girerd, *J. Am. Chem. Soc.*, 1988, **110**, 7398–7411.

8 T. K. Lal and R. Mukherjee, *Inorg. Chem.*, 1998, **37**, 2373–2382.

9 S. Mahapatra, T. K. Lal and R. Mukherjee, *Inorg. Chem.*, 1994, **33**, 1579–1580.

10 F. J. Wu, D. M. Kurtz, K. S. Hagen, P. D. Nyman, P. G. Debrunner and V. A. Vankai, *Inorg. Chem.*, 1990, **29**, 5174–5183.

11 J. E. Sheats, R. S. Czernuszewicz, G. C. Dismukes, A. L. Rheingold, V. Petrouleas, J. Stubbe, W. H. Armstrong, R. H. Beer and S. J. Lippard, *J. Am. Chem. Soc.*, 1987, **109**, 1435–1444.

12 J. B. Vincent, K. Folting, J. C. Huffman and G. Christou, *Biochem. Soc. Trans.*, 1988, **16**, 822–823.

13 J. B. Vincent, H. L. Tsai, A. G. Blackman, S. Wang, P. D. W. Boyd, K. Folting, J. C. Huffman, E. B. Lobkovsky, D. N. Hendrickson and G. Christou, *J. Am. Chem. Soc.*, 1993, **115**, 12353–12361.

14 M. Corbella, G. Fernández, P. González, M. Maestro, M. Font-Bardia and H. Stoeckli-Evans, *Eur. J. Inorg. Chem.*, 2012, **2012**, 2203–2212.

15 V. Gómez, M. Corbella and G. Aullón, *Inorg. Chem.*, 2010, **49**, 1471–1480.

16 R. Boča, *Coord. Chem. Rev.*, 2004, **248**, 757–815.

17 S. Gomez-Coca, E. Cremades, N. Aliaga-Alcalde and E. Ruiz, *J. Am. Chem. Soc.*, 2013, **135**, 7010–7018.

18 G. Aromí, J. Telser, A. Ozarowski, L.-C. Brunel, H.-M. Stoeckli-Evans and J. Krzystek, *Inorg. Chem.*, 2005, **44**, 187–196.

19 C. Duboc, D. Ganyushin, K. Sivalingam, M.-N. Collomb and F. Neese, *J. Phys. Chem. A*, 2010, **114**, 10750–10758.

20 M. Retegan, M.-N. Collomb, F. Neese and C. Duboc, *Phys. Chem. Chem. Phys.*, 2012, **15**, 223–234.

21 L. Escriche-Tur, M. Corbella, M. Font-Bardia, I. Castro, L. Bonneviot and B. Albela, *Inorg. Chem.*, 2015, **54**, 10111–10125.

22 T. Sala and M. V. Sargent, *J. Chem. Soc. Chem. Commun.*, 1978, 253–254.

23 *SADABS, Version 2008/1; Sheldrick*, Bruker AXS Inc., 2008.

24 G. M. Sheldrick, *Acta Crystallogr., Sect. A: Fundam. Crystallogr.*, 2007, **64**, 112–122.

25 A. L. Spek, *J. Appl. Crystallogr.*, 2003, **36**, 7–13.

26 P. van der Sluis and A. L. Spek, *Acta Crystallogr., Sect. A: Fundam. Crystallogr.*, 1990, **46**, 194–201.

27 G. B. Deacon and R. J. Phillips, *Coord. Chem. Rev.*, 1980, **33**, 227–250.

28 V. Gómez and M. Corbella, *Eur. J. Inorg. Chem.*, 2012, **2012**, 3147–3155.

29 N. F. Chilton, R. P. Anderson, L. D. Turner, A. Soncini and K. S. Murray, *J. Comput. Chem.*, 2013, **34**, 1164–1175.

30 O. Kahn, *Molecular magnetism*, VCH, 1993.

31 L. P. Hammett, *Trans. Faraday Soc.*, 1938, **34**, 156–165.

32 L. P. Hammett, *J. Am. Chem. Soc.*, 1937, **59**, 96–103.

33 C. Chen, H. Zhu, D. Huang, T. Wen, Q. Liu, D. Liao and J. Cui, *Inorg. Chim. Acta*, 2001, **320**, 159–166.